

WZ production in association with two jets at NLO in QCD

Francisco Campanario,^{1,*} Matthias Kerner,^{2,†} Le Duc Ninh,^{2,‡} and Dieter Zeppenfeld^{2,§}

¹*Theory Division, IFIC, University of Valencia-CSIC, E-46980 Paterna, Valencia, Spain.*

²*Institute for Theoretical Physics, KIT, 76128 Karlsruhe, Germany.*

We report on the calculation of $W^\pm Zjj$ production with leptonic decays at hadron-hadron colliders at next-to-leading order in QCD. These processes are important both to test the quartic gauge couplings of the Standard Model and because they constitute relevant backgrounds to beyond standard model physics searches. Our results show that the next-to-leading order corrections reduce significantly the scale uncertainties and have a non-trivial phase space dependence.

PACS numbers: 12.38.Bx, 13.85.-t, 14.70.Fm, 14.70.Hp

The study of di-boson production in association with two jets at the LHC is important both to test the quartic gauge couplings of the Standard Model (SM) and because they constitute relevant backgrounds to beyond standard model physics searches. At leading order (LO), there are two distinct production mechanisms. The purely electroweak (EW) contributions of the order $\mathcal{O}(\alpha^6)$ include, in particular, the four-vector-boson scatterings of the type $VV \rightarrow VV$ where the initial gauge bosons are radiated from the incoming (anti-)quarks. This “vector-boson-fusion” mechanism has been considered at next-to-leading order (NLO) in QCD for W^+W^- [1], ZZ [2], $W^\pm Z$ [3] and the equal-charge W^+W^+/W^-W^- [4, 5] production processes. In addition, there are QCD contributions of the order $\mathcal{O}(\alpha_s^2\alpha^4)$. The NLO QCD corrections to these contributions are much more difficult because QCD radiation occurs already at LO, leading to complicated topologies with non-trivial color structures at NLO. The calculations for W^+W^-jj production have been presented in Refs. [6, 7] and for the $W^+W^\pm jj$ case in Ref. [8]. In this letter, we present the first theoretical prediction for $W^\pm Zjj$ production at order $\mathcal{O}(\alpha_s^3\alpha^4)$. The interference effects between the EW and QCD amplitudes are not considered in this letter and can be neglected for a few-percent precision measurements at the LHC. This is justified because those effects are color and kinematically suppressed, since the EW and QCD contributions peak in different phase-space regions.

The leptonic decays of the EW gauge bosons are consistently included, with all off-shell effects and spin correlations taken into account. The charged leptons in the final state can stem from a Z boson or a virtual photon. All possibilities are included to form an EW and QCD gauge invariant set. Therein, the dominant contribution comes from the diagrams where both W^\pm and Z can be simultaneously on-shell. In the following, we consider the specific leptonic final state $e^+\nu_e\mu^+\mu^-$ and $e^-\bar{\nu}_e\mu^-\mu^+$. The total results for all possible decay channels (*i.e.* $e^+\nu_e\mu^+\mu^-$, $\mu^+\nu_\mu e^+e^-$, $e^+\nu_e e^+e^-$, $\mu^+\nu_\mu\mu^+\mu^-$ in the W^+Zjj case and accordingly for the W^-Zjj production) can, apart from negligible identical lepton interference effects, be obtained by multiplying our pre-

dictions by a factor four. For simplicity, we choose to describe the resonating W^\pm and Z propagators with a fixed width and keep the weak-mixing angle real.

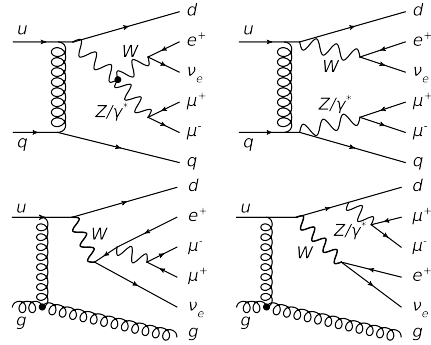


FIG. 1: Representative tree-level Feynman diagrams.

The amplitudes are obtained using the Feynman-diagrammatic approach. At LO, all contributions to, for example, $pp \rightarrow e^+\nu_e\mu^+\mu^-jj$ are classified into two groups, 4-quark and 2-quark-2-gluon amplitudes, as depicted in Fig. 1. Each group is then further divided into two QCD-gauge-invariant sub-groups (i) with two EW gauge bosons coupling to the quark lines and (ii) with the W^\pm radiated from a quark line decaying into four leptons. Crossing symmetry is used to obtain all 90 subprocesses from the minimal set of five generic subprocesses, for two generations of quarks. At NLO, there are the virtual and the real corrections. Fig. 2 shows some selected contributions to the virtual amplitude, which involves in particular the hexagon diagrams. The most difficult part of the calculation is computing the 2-quark-2-gluon virtual amplitudes with up to six-point rank-five one-loop tensor integrals. There are 84 six-point diagrams for each of seven independent subprocesses. The 4-quark group is much easier with only 12 hexagons for the most complicated subprocesses with same-generation quarks. The calculation of tensor integrals is done by using Passarino-Veltman reduction [9] for up to 4-point diagrams and the method of Ref. [10] (see also Ref. [11]) for higher-point tensor integrals. The scalar integrals are calculated as in Refs. [12–14]. The real emission contri-

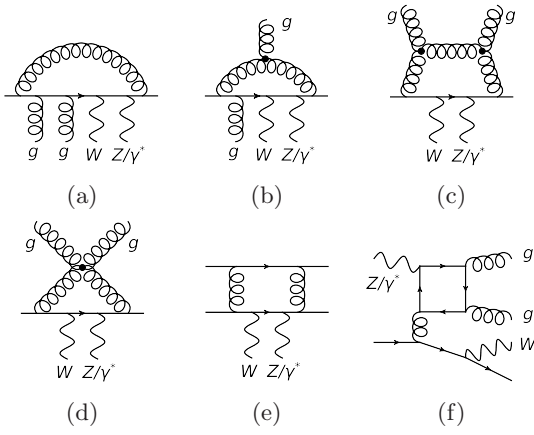


FIG. 2: Selected Feynman diagrams contributing to the virtual amplitudes.

bution includes, for two generations of quarks, 146 subprocesses with seven particles in the final state. Both the virtual and real corrections are, apart from the UV divergences in the virtual amplitude which are removed by the renormalization of α_s , separately infrared divergent. These divergences cancel in the sum for infrared-safe observables such as the inclusive cross section and jet distributions. We use the dimensional regularization method [15] to regularize the UV and the infrared divergences and apply the Catani-Seymour dipole subtraction algorithm [16] to combine the virtual and the real contributions.

We have constructed two independent implementations of the above described method. The results of the two computer codes are in full agreement, typically 8 to 12 digits with double precision, at the amplitude level for all subprocesses at NLO. The integrated part of the dipole subtraction term in Ref. [16] has been compared at the integration level. Moreover, we have also simplified the calculation to compare with MCFM [17, 18] for the case of $e^+\nu_e jj$ production at NLO and found agreement at the per mille level. The first implementation is done in the VBFNLO framework [19], which will be described below. The second implementation uses **FeynArts-3.4** [20] and **FormCalc-6.2** [21] to obtain the virtual amplitudes. The scalar and tensor one-loop integrals are evaluated with the in-house library **LoopInts**. The tree-level amplitudes for both LO and NLO real emission contributions are calculated in an optimized way by using **HELAS** [22, 23] routines.

In the following, we sketch the main implementation which has been added to the VBFNLO program and will be made public. We use the spinor-helicity formalism of Ref. [24]. The virtual amplitudes are constructed using generic building blocks, which include sets of loop corrections to Born topologies with a fixed number and a fixed order of external particles. For example, by starting from the diagram in Fig. 2a, we can form a building

block by attaching the virtual gluon in all possible ways to the quark line, thereby including also pentagon, box, triangle and self energy corrections. Within the building blocks, an appropriate color factor is assigned to each Feynman diagram. Because the building blocks assume the polarization vector of the external gauge bosons as an effective current and do not use special properties like transversality or being on-shell, they can be also used to check various identities relating N -point integrals to lower point integrals by replacing a polarization vector with the corresponding momentum. Those identities are called gauge tests and are checked for every phase space point with a small additional computing cost by using a cache system. This is important because the phase space integration of the virtual contribution shows numerical instabilities in the calculation of one-loop tensor integrals. If a bad phase-space point is identified, *i.e.* the gauge tests are true by less than 2 digits with double precision, the program then calculates the associated building blocks again with quadruple precision. The gauge tests are applied again and the point is discarded if they fail. For a typical calculation with the inclusive cuts specified below the number of discarded points is statistically negligible. This strategy was also successfully applied for $W\gamma\gamma + \text{jet}$ at NLO QCD in Ref. [25]. Further details about the building blocks, tensor reduction master equations and the issue of numerical instabilities can be found in Ref. [26] and also in a forthcoming publication. Since the leptonic decays of the EW gauge bosons are common for all subprocesses, the VBFNLO approach is to calculate these decays once for each phase-space point and store them. Due to the large number of subprocesses, we extend this procedure and also precalculate parts of Feynman diagrams, that are common to the subprocesses of the real emission. In addition, a caching system to reuse Born amplitudes for different dipole terms [16] has been implemented. With this method, we obtain the NLO inclusive cross section with statistical error of 1% in 2.5 hours on an Intel i5-3470 computer with one core and using the compiler Intel-ift version 12.1.0.

We use $M_Z = 91.1876 \text{ GeV}$, $M_W = 80.385 \text{ GeV}$ and $G_F = 1.16637 \times 10^{-5} \text{ GeV}^{-2}$ as EW input parameters and derive the weak-mixing angle from the SM tree-level relations. All fermions but the top quark are approximated as massless. The widths are calculated as $\Gamma_W = 2.09532 \text{ GeV}$, $\Gamma_Z = 2.50606 \text{ GeV}$. The MSTW2008 parton distribution functions (PDF) [27] with $\alpha_s^{\text{LO}}(M_Z) = 0.13355$ and $\alpha_s^{\text{NLO}}(M_Z) = 0.11490$ are used. The numerical results presented in this letter are calculated in the four-flavor scheme (*i.e.* the third-generation quarks are excluded in the calculation of the α_s running, the PDF evolution and the amplitudes of the hard processes) for the LHC at 14 TeV center-of-mass energy. This choice is justified because the external b -quark contribution can, in principle, be excluded by using b tagging. The results for the five-flavor scheme will be presented elsewhere. Effects

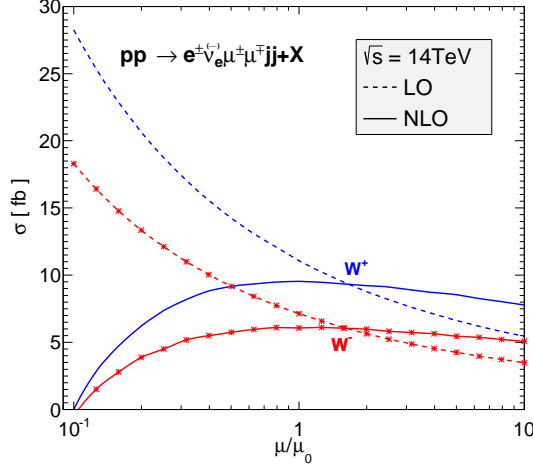


FIG. 3: Scale dependence of the LO and NLO cross sections at the LHC. The curves with and without stars are for W^-Zjj and W^+Zjj productions, respectively.

from generation mixing are neglected. To have a large phase space for QCD radiation, we choose inclusive cuts. The charged leptons are required to be hard and central: $p_{T,\ell} \geq 20$ GeV and $|y_\ell| \leq 2.5$. The missing transverse energy must satisfy the cut $E_{T,\text{miss}} \geq 30$ GeV. For any pair of opposite-charge leptons, we impose $m_{\ell\ell} \geq 15$ GeV, which avoids collinear singularities coming from off-shell photons $\gamma^* \rightarrow \ell^+\ell^-$. All final state partons are clustered to jets by using the anti- k_t algorithm [28] with the radius $R = 0.4$. There must be at least two hard jets with $p_{T,\text{jet}} \geq 20$ GeV and $|y_{\text{jet}}| \leq 4.5$. In addition, we impose a requirement on the lepton-lepton and lepton-jet separation in the azimuthal angle-rapidity plane $\Delta R_{\ell(j)} \geq 0.4$, where only jets passing the above cuts are involved. As the central value for the factorization and renormalization scales, we choose $\mu_F = \mu_R = \mu_0 = (\sum_{\text{jet}} p_{T,\text{jet}} + \sqrt{p_{T,W}^2 + m_W^2} + \sqrt{p_{T,Z}^2 + m_Z^2})/2$, where $p_{T,V}$ and m_V with V being W or Z are understood as the reconstructed transverse momenta and invariant masses of the decaying bosons and the sum includes only jets passing all cuts.

Since the results are calculated at a fixed order in perturbative QCD, they depend on the arbitrary scales μ_F and μ_R . The validity of the theoretical predictions is established by proving that the scale dependence reduces when higher-order terms are included. This is shown in Fig. 3 for the cross section calculated at LO and NLO. For simplicity, the two scales are set equal. As expected, we observe a significant reduction in the scale dependence around the central value μ_0 when the NLO contribution is included. For both W^+ and W^- cases, the uncertainties obtained by varying $\mu_{F,R}$ by factors 1/2 and 2 around the central value are 50% at LO and 5% at NLO. At $\mu = \mu_0$, we get $\sigma_{\text{LO}} = 11.1^{+3.2}_{-2.3}$ fb ($7.1^{+2.0}_{-1.5}$ fb) and $\sigma_{\text{NLO}} = 9.5^{+0.0}_{-0.4}$ fb ($6.1^{+0.0}_{-0.3}$ fb) for the $W^+(W^-)$ case.

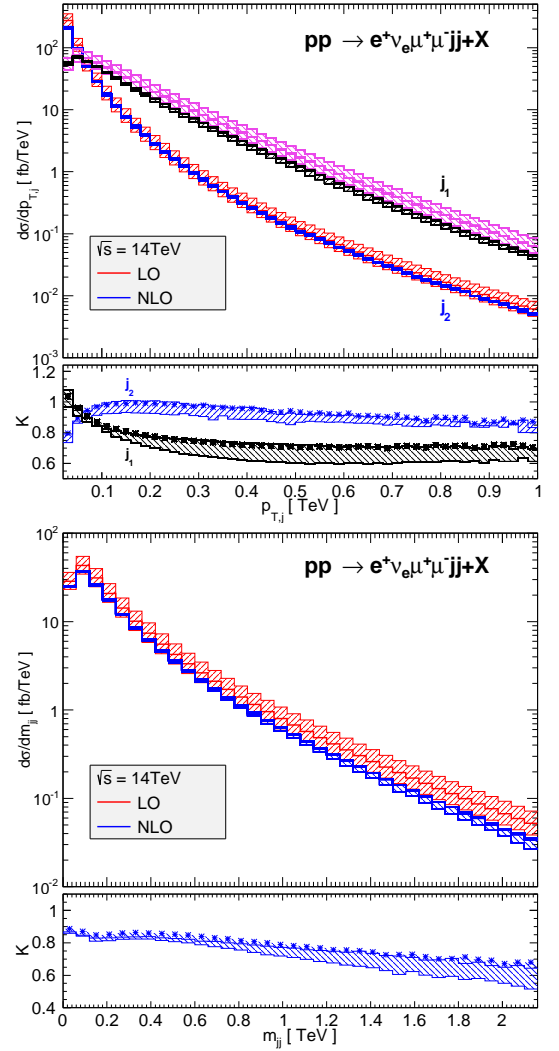


FIG. 4: Differential cross sections and K factors for the transverse momenta (top) and the invariant mass (bottom) of the two hardest jets. The bands describe $\mu_0/2 \leq \mu_F = \mu_R \leq 2\mu_0$ variations. The K -factor bands are due to the scale variations of the NLO results, with respect to $\sigma_{\text{LO}}(\mu_0)$. The curves with stars in the lower panels are for the central scale, while the two solid lines correspond to $\mu_F = \mu_R = 2\mu_0$ and $\mu_0/2$.

At LO, the dominant contribution is from the 2-quark-2-gluon group, about 86% for both cases. By varying the two scales separately, we observe a small dependence on μ_F , while the μ_R dependence is similar to the behavior shown in Fig. 3.

We show the distributions of the transverse momenta and the invariant mass of the two hardest jets in Fig. 4, and the transverse mass of the two gauge bosons $m_{T,WZ}$ in Fig. 5. We define, as in Ref. [29], $m_{T,WZ}^2 = (\sqrt{m^2(\ell\ell) + p_T^2(\ell\ell)} + |p_{T,\text{miss}}|)^2 - (\vec{p}_T(\ell\ell) + \vec{p}_{T,\text{miss}})^2$, with $m(\ell\ell)$ and $p_T(\ell\ell)$ denoting the invariant mass and transverse momentum of the charged-lepton system, re-

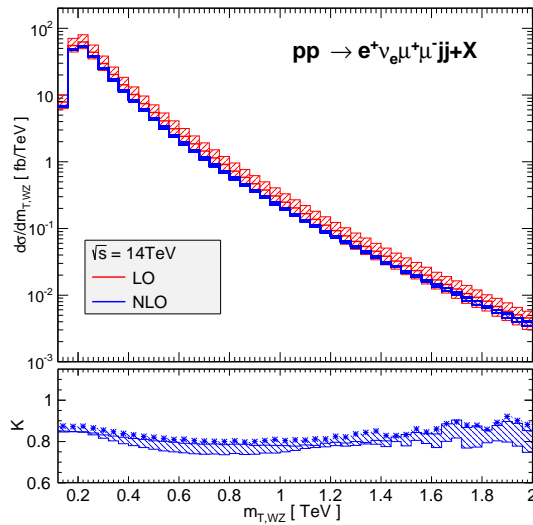


FIG. 5: Similar to Fig. 4 but for the transverse mass of the two gauge bosons $m_{T,WZ}$.

spectively. The K factors, defined as the ratio of the NLO to the LO results, are shown in the lower panels. The distributions at NLO are much less sensitive to the variation of the scales than at LO. The K factors vary from 0.6 to 1 in a large energy range. This fact together with Fig. 3 indicate that we should choose a larger central scale, about $2\mu_0$, to bring the LO results closer to the NLO ones for the inclusive cuts. We have also studied a fixed scale choice such as $\mu_0^{\text{fix}} = 400 \text{ GeV}$ and found that the NLO inclusive cross section as a function of the scales is stable around μ_0^{fix} and is close to the LO one as well as the dynamic scale prediction. However, the transverse momentum and the invariant mass distributions become unstable at large p_T , with very small K factors. This is because the bulk of the inclusive cross section comes from the low energy regime as shown in Fig. 4 and Fig. 5, but a fixed energy scale is not appropriate for all energy regimes. The steep increase of the K factor for the transverse momentum distribution of the second hardest jet near 20 GeV is probably a threshold effect: the phase space for three-visible-jet events is opened up as p_{T,j_2} grows well above the cut of 20 GeV.

In this letter, we have reported on the first calculation of $W^\pm Z jj + X$ production at order $\mathcal{O}(\alpha_s^3 \alpha^4)$ and found K factors close to one. While further phenomenological results will be presented in a future paper, we also plan to make the code publicly available as part of the VBFNLO program [19].

We acknowledge the support from the Deutsche Forschungsgemeinschaft via the Sonderforschungsbereich/Transregio SFB/TR-9 Computational Particle Physics. FC is funded by a Marie Curie fellowship (PIEF-GA-2011-298960) and partially by MINECO (FPA2011-23596) and by LHCPHENONET (PITN-

GA-2010-264564). MK thanks the “Strukturiertes Promotionskolleg in KCETA” for financial support.

* francisco.campanario@ific.uv.es

† matthias.kerner@kit.edu

‡ duc.le@kit.edu

§ dieter.zeppenfeld@kit.edu

- [1] B. Jäger, C. Oleari, and D. Zeppenfeld, JHEP **0607**, 015 (2006).
- [2] B. Jäger, C. Oleari, and D. Zeppenfeld, Phys.Rev. **D73**, 113006 (2006).
- [3] G. Bozzi, B. Jäger, C. Oleari, and D. Zeppenfeld, Phys.Rev. **D75**, 073004 (2007).
- [4] B. Jäger, C. Oleari, and D. Zeppenfeld, Phys.Rev. **D80**, 034022 (2009).
- [5] A. Denner, L. Hosekova, and S. Kallweit, Phys.Rev. **D86**, 114014 (2012).
- [6] T. Melia, K. Melnikov, R. Rontsch, and G. Zanderighi, Phys.Rev. **D83**, 114043 (2011).
- [7] N. Greiner *et al.*, Phys.Lett. **B713**, 277 (2012).
- [8] T. Melia, K. Melnikov, R. Rontsch, and G. Zanderighi, JHEP **1012**, 053 (2010).
- [9] G. Passarino and M. Veltman, Nucl.Phys. **B160**, 151 (1979).
- [10] A. Denner and S. Dittmaier, Nucl.Phys. **B734**, 62 (2006).
- [11] T. Binoth, J. P. Guillet, G. Heinrich, E. Pilon, and C. Schubert, JHEP **0510**, 015 (2005).
- [12] G. 't Hooft and M. Veltman, Nucl.Phys. **B153**, 365 (1979).
- [13] S. Dittmaier, Nucl.Phys. **B675**, 447 (2003).
- [14] A. Denner and S. Dittmaier, Nucl.Phys. **B844**, 199 (2011).
- [15] G. 't Hooft and M. Veltman, Nucl.Phys. **B44**, 189 (1972).
- [16] S. Catani and M. Seymour, Nucl.Phys. **B485**, 291 (1997).
- [17] J. M. Campbell and R. K. Ellis, Phys.Rev. **D65**, 113007 (2002).
- [18] J. M. Campbell, R. K. Ellis, and D. L. Rainwater, Phys.Rev. **D68**, 094021 (2003).
- [19] K. Arnold *et al.*, Comput.Phys.Comm. **180**, 1661 (2009).
K. Arnold *et al.*, (2012), arXiv:1207.4975.
- [20] T. Hahn, Comput.Phys.Comm. **140**, 418 (2001).
- [21] T. Hahn and M. Perez-Victoria, Comput. Phys. Commun. **118**, 153 (1999).
- [22] H. Murayama, I. Watanabe, and K. Hagiwara, (1992).
- [23] J. Alwall *et al.*, JHEP **0709**, 028 (2007).
- [24] K. Hagiwara and D. Zeppenfeld, Nucl.Phys. **B313**, 560 (1989).
- [25] F. Campanario, C. Englert, M. Rauch, and D. Zeppenfeld, Phys.Lett. **B704**, 515 (2011).
- [26] F. Campanario, JHEP **1110**, 070 (2011).
- [27] A. Martin, W. Stirling, R. Thorne, and G. Watt, Eur.Phys.J. **C63**, 189 (2009).
- [28] M. Cacciari, G. P. Salam, and G. Soyez, JHEP **0804**, 063 (2008).
- [29] C. Englert, B. Jäger, M. Worek, and D. Zeppenfeld, Phys.Rev. **D80**, 035027 (2009).